

Photophysics and Dynamics of Surface Plasmon Polaritons-Mediated Energy Transfer in the Presence of an Applied Electric Field

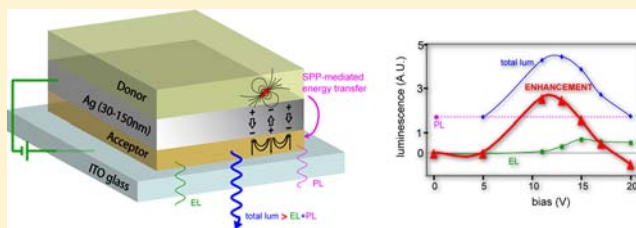
Elisabetta Collini,^{*,†} Francesco Todescato,[†] Camilla Ferrante,[†] Renato Bozio,[†] and Gregory D. Scholes[‡]

[†]Department of Chemical Sciences and INSTM, University of Padova, Via Marzolo 1, I-35131 Padova, Italy

[‡]Department of Chemistry, University of Toronto, 80 St George Street, Toronto, ON M5S3H6, Canada

S Supporting Information

ABSTRACT: The possibility to transfer energy between molecular excitons across a metal film up to 150 nm thick represents a very attractive solution to control and improve the performances of thin optoelectronic devices. This process involves the presence of coupled surface plasmon polaritons (SPPs) at the two dielectric–metal interfaces, capable of mediating the interactions between donor and acceptor, located on opposite sides of the metal film. In this Article, the photophysics and the dynamics of an efficient SPP-mediated energy transfer between a suitable dye and a conjugated polymer is characterized by means of steady-state and time-resolved photoluminescence techniques. The process is studied in model multilayer structures (donor/metal/acceptor) as well as in electrically pumped heterostructures (donor/metal cathode/acceptor/anode), to verify the effects of applied electric fields on the efficiency and the dynamics of SPP-mediated energy transfer. A striking enhancement of the overall luminescence was recorded in a particular range of applied bias, suggesting the presence of cooperative effects between optical and electrical stimulations.



1. INTRODUCTION

The study of mechanisms and dynamics of energy transfer (ET) in systems of increasing complexity has been one of the most popular research topics in the past decades, because of the crucial role played by ET in many natural and artificial processes.^{1–3} In past years, the literature has reported several different approaches to maximize the efficiency of the process and make it suitable for applications in real devices. One of the most fascinating approaches in this regard is the use of plasmonic phenomena.⁴ In particular, it was recently demonstrated that long distance ET is achieved, far beyond the Förster radius, in multilayer structures where the donor and the acceptor moieties are located on the opposite interfaces of a thin metal film. This is due to the presence of coupled surface plasmon polaritons (SPPs)⁵ at the two dielectric–metal interfaces, capable of mediating the donor–acceptor interaction.⁶ In this Article, SPP-mediated ET (SPP-ET) from a molecular donor to a conjugated polymer acceptor is studied. Our main finding is that not only the energy can be efficiently transported from the donor to acceptor for distances up to 150 nm, but also that the presence of an electric field can cooperatively enhance the process.

This SPP-ET is different from the conventional Förster energy transfer. In the Förster mechanism, the excitation energy is transferred in a nonradiative way through the resonant dipole–dipole interaction between donor and acceptor. The nature of such an interaction limits the Förster radius, defined as a critical ET distance, to a range of 1–10 nm.⁷ Instead, the SPP-ET mechanism involves an efficient coupling of the near-

fields of donor and acceptor dipole moments to the SPP modes of the metal: the donor molecular excitons resonantly excite surface plasmon modes on both sides of the optically thick metal layer, which evanescently couple to acceptor molecules on the other interface. Because SPP modes extend deeply into both dielectric layers, the range of ET can be extended up to hundreds of nanometers. In addition, they propagate in the plane of the metal layer rather than parallel to the incident radiation, thereby providing a more efficient mean of pumping plane structures.

The overall process presents a nontrivial mechanism that goes beyond the conventional classification in radiative or nonradiative transfer, typically invoked to describe ET between organic dyes.^{8,9} The migration of the energy across the metal film (Figure 1) can be indeed described as: (i) conversion of the oscillating transition dipole of the initially excited antenna donor into surface charge-density waves in the first metal–dielectric interface; (ii) cross coupling of the two surface plasmons on the opposite interfaces of the metal film; and finally (iii) transfer of excitation energy to the acceptor on the second metal–dielectric interface. The phenomenon is analogous to the evanescent-wave coupling, a process by which electromagnetic waves are transmitted from one medium to another by means of the evanescent, exponentially decaying electromagnetic field.¹⁰

Received: February 13, 2012

Published: May 22, 2012

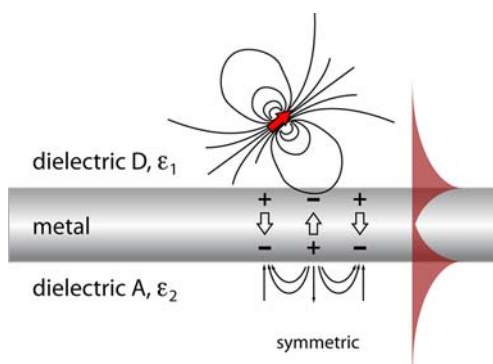


Figure 1. Schematic representation of the energy transfer through a metal film mediated by surface plasmon polaritons. In this sketch, only the coupling with the symmetric mode is shown.

The behavior of an excited fluorophore nearby a metal surface (step i) is deeply studied in the literature.^{11–15} In particular, the transfer of energy from the oscillating transition dipole of the fluorophore to surface plasmons at the metal–dielectric interface was proved to be the main relaxation process for molecules at distances up to 400 nm from the interface.¹⁵ This relaxation process is now recognized as the main cause of fluorescence quenching of dyes in proximity of metallic surfaces. The oscillating transition dipole of the initially excited donor molecule can be treated as a quantum-mechanical antenna, which drives electronic charge-density oscillations on the metal–dielectric interface, by its electromagnetic field. When the electronic transition frequency and the surface plasmon frequency are nearly degenerate, the localized electronic energy of the dipole can be effectively converted into surface charge-density waves in the metal surface: a plasmon polariton is now created at the metal–dielectric interface, characterized by an exponentially decaying field inside the metal film.¹³

If the thickness of the metal film is thin enough so that the evanescent tails of the respective modes show considerable overlap, then the SPP mode created at the first interface can couple with a plasmon polariton mode at the other interface (step ii). The coupling results in two mixed modes exhibiting dispersion with film thickness. Specifically, the usual symmetric and antisymmetric branches each split into a pair of waves, one radiative and the other nonradiative.¹⁶ The evanescent field decays exponentially in the adjacent dielectric medium with a penetrating depth of approximately 100 nm. The evanescent wave associated with the plasmon polariton mode at the second interface can then excite a fluorescent probe (acceptor) on the other side of the metal film with respect to the excited donor (step iii). The possibility to transfer energy from a surface plasmon mode, excited in a suitable configuration, to fluorophores located near the metal–dielectric interface is the basic principle of surface plasmon fluorescence spectroscopy,^{15,17,18} and it is now largely exploited in the sensing and biosensing field.^{15,19}

Despite the noteworthy potential of this process, only a few experimental tests were done since the original paper by Andrew and Barnes⁶ in 2004, and few applications were proposed.²⁰ This is probably because, although the coupling between the donor dipole moment and the SPP mode is highly efficient (>95%),¹¹ the ET efficiency is not guaranteed to be as high. In the original work of Andrew and Barnes, indeed, the peak efficiency of the SPP-ET was approximately 5%,⁶ too small

for most applications. However, more recent results suggest that a careful design of the sample structure could in principle improve this value by an order of magnitude.²¹

To our knowledge, SPP-ET was exploited to improve the top emission from organic light-emitting devices (OLEDs)^{22,23} and to enhance the optical absorption of organic photovoltaics (OPVs).²¹

In view of such applications, major efforts have been devoted to find new strategies to enhance the overall SPP-ET efficiency, for example, optimizing the device design²¹ or increasing the cross coupling of the two surface plasmons on the opposite interfaces employing corrugated metal films²² or 2D nanowire arrays.²⁴

Less attention has been dedicated to the study of the effects of electric fields on the SPP-ET mechanism and efficiency at the microscopic level. This is a rather crucial aspect in an attempt to increase the performances of devices through SPP-ET processes, because the presence of electric fields in working devices can seriously affect the photophysics and the dynamics of the process.

This Article aims to fill this gap, focusing the attention on the study of the combined effect of optical and electrical stimulation in multilayer structures supporting SPP-ET. To this aim, SPP-ET between suitable dyes and a conjugated polymer (poly[2-methoxy-5-(2'-ethyl-hexyloxy)-1,4-phenylene vinylene], MEH-PPV) on the opposite faces of an Ag film is studied and characterized by means of time-resolved fluorescence techniques.

2. EXPERIMENTAL SECTION

2.1. Samples Preparation. Preliminary studies on SPP-ET were performed on model multilayer structures consisting of donor and acceptor thin films on a glass substrate, separated by a silver film thick enough to prohibit conventional Förster-type ET processes. The data reported in this Article refer to multilayer samples with structure glass/acceptor/Ag/donor, where the acceptor is the conjugated polymer poly[2-methoxy-5-(2'-ethyl-hexyloxy)-1,4-phenylene vinylene] (MEH-PPV) and the donor is 9,10-diphenylanthracene (DPA). Other combinations of dyes were considered (see the Supporting Information), but the pair DPA/MEH-PPV resulted to be the most efficient for our purposes. To prepare the multilayer samples, a chlorobenzene solution of MEH-PPV (Sigma Aldrich, $M_n \approx 70\,000$ – $100\,000$) was spun directly on the glass substrate to form a film of about 80 nm. Ag films with thicknesses between 30 and 150 nm were then thermally grown on top of the acceptor layer (rate 1 Å/s) and capped with an 80 nm thick donor film obtained by thermal evaporation of DPA (rate 0.1 Å/s). Identical donor-only [glass/Ag/DPA] and acceptor-only [glass/MEH-PPV/Ag] reference samples were also fabricated with the same procedure.

To study the effect of the application of an electric field on the SPP-ET efficiency, prototype electrically pumped heterostructures (EPHs) were prepared, based on the conventional structure of a single-layer MEH-PPV OLED. EPHs were fabricated with the same aforementioned procedure, substituting the glass substrate with ITO glass (Visiotek, ITO OLED graded 15 Ω/□) covered with a commercial PEDOT:PSS (Sigma Aldrich) thin film obtained by spin-coating. The final prototype devices had a structure: glass/ITO(150 nm)/PEDOT:PSS(80 nm)/MEH-PPV(80 nm)/Ag(90 nm)/DPA(80 nm). In these multilayers, the Ag film has the dual function of metal cathode and plasmonic substrate for SPP-ET.

2.2. Spectroscopic Methods. The linear optical properties of MEH-PPV and DPA films on glass were preliminarily characterized recording the absorption and fluorescence spectra on a Cary 5 spectrophotometer and a Fluoromax (Spex Jobin Yvon) fluorimeter, respectively.

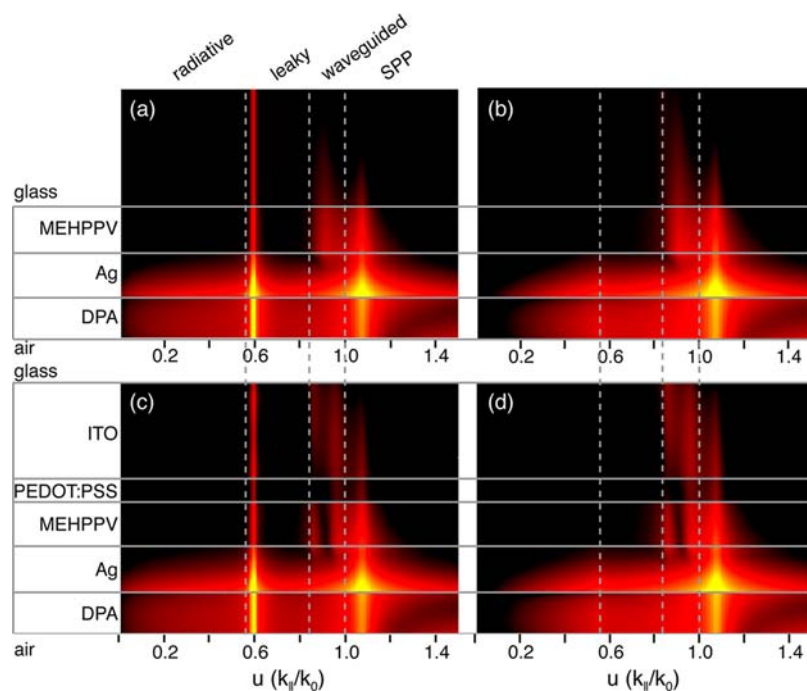


Figure 2. Absorption of the parallel (a) and perpendicular (b) emitting dipole energy as a function of the position and normalized surface-parallel vector ($k_{\parallel}/k_{0,DPA}$) for a model multilayer structure. Analogous results were obtained in an electrically pumped heterostructure, both for parallel (c) and for perpendicular (d) emitting dipole components. All of the panels are reported in a logarithmic color scale. In both structures, the emitting dipole is located at the middle of the DPA layer, and the emission wavelength is 500 nm. Bright features correspond to higher absorption. Perpendicular dashed lines divide the wavevector axis into air-coupled ($u < 0.56$), leaky ($0.56 < u < 0.84$), glass-waveguided ($0.84 < u < 1$), and surface plasmon polaritons ($u > 1$) regions.

Photoluminescence (PL) spectra of multilayer samples (glass/MEH-PPV/Ag, glass/Ag/DPA, and glass/MEH-PPV/Ag/DPA) were recorded with a fiber coupled spectrometer/charge-coupled device system with spectral resolution of 1 nm (Ocean Optics). Excitation was provided by a frequency doubled Ti:sapphire fs laser system (400 nm, 76 MHz, 100 fs). The pump wavelength was tuned to an absorption maximum of DPA spectrum to minimize direct excitation of MEH-PPV. Samples were pumped from the DPA side and PL was collected from the opposite side (glass side).

Time-resolved photoluminescence (TRPL) measurements were carried out using the time-correlated single-photon counting (TCSPC) method. The experimental apparatus is based on a scanning confocal microscope (Olympus IX-71) coupled with a TimeHarp 200 TCSPC card (PicoQuant) and a single-photon counting avalanche photodiode (SPAD, MPD, Italy). The same frequency-doubled Ti:Sapphire laser was used as excitation source. The excitation beam, suitably attenuated by means of neutral density filters, was focused by a 20 \times microscope objective into the upper donor layer. Fluorescence is collected by the same microscope objective, passed through a dichroic mirror, and focused through a pinhole (150 μ m), to reject out-of-focus light. Appropriate band-pass filters were employed in front of the SPAD to select the fluorescence wavelength range. In these experimental conditions, the axial resolution (fwhm) is approximately 6 μ m. The instrument response function (IRF) of the whole apparatus has a fwhm of about 150 ps, determined by means of scattered light detection. The samples were pumped from the top DPA layer, and the ensuing PL from MEH-PPV was collected from the same side. The same excitation geometry was applied also to the control donor-only and acceptor-only samples.

3. SIMULATIONS

To examine and quantify the efficiency of ET within multilayer stacks, preliminary simulations were undertaken to find the optimal donor–acceptor pair and the best multilayer design. ET within the multilayer structure was modeled following the

analytical method developed by Celebi et al.²⁵ Briefly, exciton decay rate and electric field distribution are calculated using a classical dipole model¹⁴ and dyadic Green's functions approach.²⁶ The energy flux is then obtained evaluating the Poynting vector, which is readily formulated using these dyadic functions. The model allows calculating the energy flux through each interface and thus estimating the amount of energy absorbed by each layer as the difference of the incoming and outgoing fluxes. In this way, it is possible to visualize how the initial energy of the emitting dipole placed in the donor layer couples with the adjacent metal surface and how it flows through the multilayer structure.

Figure 2 shows the results of the simulation performed on the following structures: glass/MEH-PPV(80 nm)/Ag(80 nm)/DPA(80 nm) (panels a and b) and glass/ITO/PEDOT:PSS/MEH-PPV(80 nm)/Ag(80 nm)/DPA(80 nm) (panels c and d). In the calculation, the emission wavelength is set to 500 nm, and the emitting dipole is placed at the center of DPA layer. Following the formalism described in ref 14, the parallel (\parallel) and the perpendicular (\perp) components of the oscillating dipole with respect to the film surface are treated separately and shown in different panels of Figure 2. For an isotropic distribution of dipole configurations, the total energy absorption (E_{iso}) can be easily calculated as $E_{iso} = 1/3E_{\perp} + 2/3E_{\parallel}$. The input parameters are the complex frequency-dependent dielectric functions $\epsilon(\omega)$ and the thickness of each layer. The $\epsilon(\omega)$ of silver, glass, and PEDOT:PSS was obtained from literature data.²⁵ For MEH-PPV and DPA films, the real part of $\epsilon(\omega)$, connected with the refractive index, was obtained from literature data,^{27,28} whereas the imaginary part, related to the absorption coefficient, was extracted from linear absorption spectra.

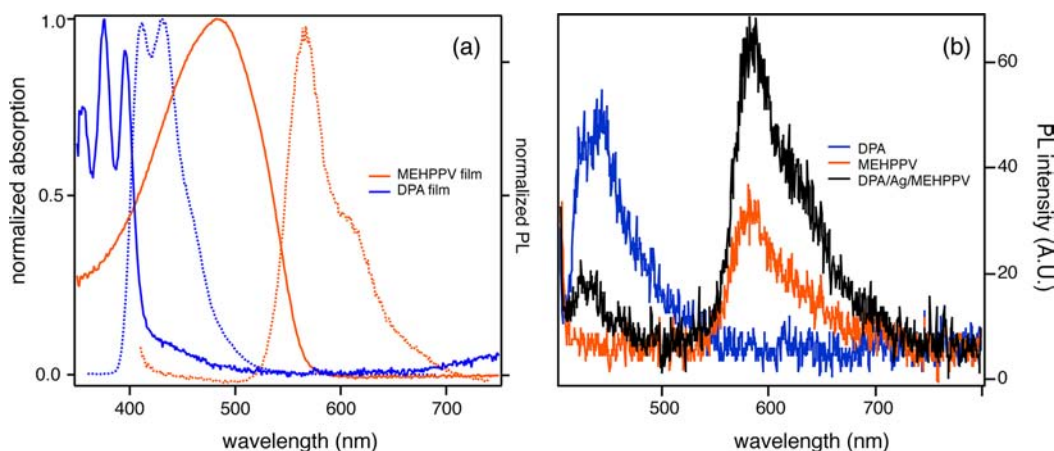


Figure 3. (a) Normalized absorption (solid lines) and emission (dotted lines) of an 80 nm thick DPA film (blue) and an 80 nm thick MEH-PPV film (orange) deposited on a glass substrate. (b) PL spectra from donor-only (DPA/Ag/glass, blue), acceptor-only (Ag/MEH-PPV/glass, orange), and complete donor–acceptor structures (DPA/Ag/MEH-PPV/glass, black).

In the figure, the migration of energy from the source donor layer (DPA) to the final acceptor layer (MEH-PPV) through the metal film is represented plotting the percentage of this initial energy absorbed by each layer, calculated taking the difference of the magnitude of the incoming and outgoing energy flux at both boundaries of the layer. The absorbed energy associated with the parallel and perpendicular components of the emitting dipoles is plotted separately as a function of the normalized surface parallel wavevector u , defined as $(k_{\parallel}/k_{0,\text{DPA}})$. k_{\parallel} is the amplitude of the parallel component (with respect to the layers surface) of the propagation vector k of the electric field associated with the oscillating dipole, whereas $k_{0,\text{DPA}}$ is the wave vector magnitude in the donor antenna layer. It has been demonstrated that this normalization significantly simplifies the calculation.²⁵

To analyze the physical meaning of the different features appearing in Figure 2, it is convenient to divide the x -axis into different regions as indicated by the vertical dashed lines. Normalized wave vectors with $u < 1$ correspond to radiative modes, while those with $u > 1$ correspond to nonradiative transfer to the metal followed by energy transfer via SPPs. This can be easily verified considering the typical dispersion curve of SPPs and expressing the wavevector amplitudes in the j th layer as $k_{\parallel,j} \approx \omega \sqrt{\epsilon_j}/c$ in the calculation of u .²⁵ The fulfillment of the condition $u = k_{\parallel,\text{metal}}/k_{0,\text{DPA}} > 1$ is indeed necessary to excite an SPP at the interface.²⁹

Among radiative modes, considering the ratios between refractive indexes of adjacent layers, three regions can be further individuated. The region from $u = 0.84$ ($\sim(\epsilon_{\text{glass}}(\omega)/\epsilon_{\text{DPA}}(\omega))^{1/2}$) to $u = 1$ contains the wavevectors that are guided in the glass (and in the ITO layer, if present), whereas from $u = 0.56$ ($\sim 1/(\epsilon_{\text{DPA}}(\omega))^{1/2}$) to $u = 0.84$ wavevectors that outcouple into air are involved. These modes are usually classified as “leaky modes”.^{29,30}

The most interesting feature for our purposes is however the signal appearing at $u = 1.1$, corresponding to an SPP mode that dominates the absorption maps. The signal spans the whole multilayer sample, being strongly evident in both the silver and the acceptor layer. This means that the dipole energy initially settled in the DPA donor layer is efficiently transferred to the metal film, where an SPP mode is excited ($k_{\parallel,\text{metal}} > k_{0,\text{DPA}}$ corresponding to $u (=k_{\parallel,\text{metal}}/k_{0,\text{DPA}}) > 1$). The dipole energy is not completely dissipated in the silver film, but it partially

reaches the acceptor layer where it is absorbed. The net result is thus the transfer of excitation energy from DPA to MEH-PPV layer through the silver film. As was already noticed for other devices, the coupling to SPP modes is best for perpendicular dipoles, whereas parallel dipoles outcouple better into air.²⁵

The efficiency of such transfer process can be estimated calculating the fraction of the initial dipole energy effectively reaching the acceptor layer and being absorbed by MEH-PPV. For the structures simulated in Figure 2, such efficiency is calculated to be about 20%. As expected, the efficiency of ET was found to be critically dependent on the thickness of the metal layer, because a thick silver stratum completely dissipates the dipole energy before it could reach the acceptor layer.

In fact, the transfer efficiency has a complex dependence on metal thickness, due to a different dispersion and attenuation of symmetric and antisymmetric branches, in turn strictly connected with the dielectric constants of the media surrounding the metal (ϵ_1 and ϵ_2 in Figure 1).¹² Great attention must thus be paid also in matching such dielectric constants (in particular the refractive indexes). If the two constants are too different, the coupling between the two plasmon modes at the two metal interfaces is less efficient and the energy is dissipated at the first interface rather than transferred to the opposite one. Other parameters playing an obvious role in the process efficiency are the fluorescence quantum yield of the donor and the overlap between the donor emission and the acceptor absorption. This overlap can be optimized choosing suitable donor–acceptor pair, like for the optimization of a conventional ET process.

A closer look at Figure 2 allows also recognizing that the results obtained for the two analyzed structures are quite similar, confirming that the presence of ITO and PEDOT:PSS layers in EPHs does not perturb the photophysics of the SPP-ET. Therefore, the simple [glass/acceptor/metal/donor] structure is a good model system to study and check the efficiency of the SPP-ET also for more complicated multilayer structures.

4. EXPERIMENTAL RESULTS

4.1. SPP-ET Efficiency. Figure 3a shows the normalized absorption and PL spectra of donor (DPA) and acceptor (MEH-PPV) films on a glass substrate. The spectra show the typical features of films of the two species (for MEH-PPV, see refs 31–34; for DPA, see refs 35–38).

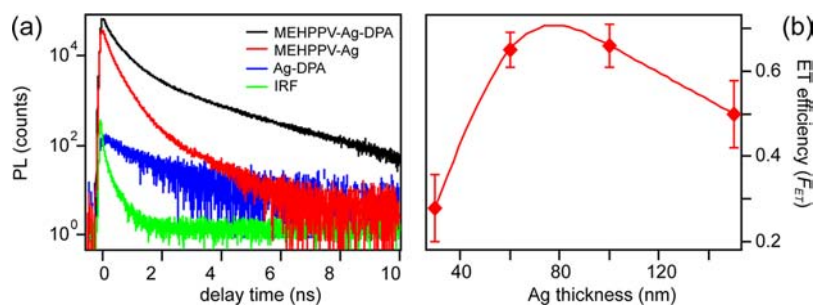


Figure 4. (a) Time-resolved PL (in log scale) of a multilayer sample with an Ag thickness of 60 nm measured in the spectral region dominated by MEH-PPV emission ($\lambda > 610$ nm). The decay recorded for the donor–acceptor MEH-PPV/Ag/DPA film (black line) is reported together with the control samples containing donor-only (Ag/DPA, blue line) and acceptor-only (MEH-PPV/Ag, red line). IRF (green line) is also reported for comparison. (b) Efficiency of the SPP-ET as a function of metal thickness, calculated in terms of fraction of the total emission due to SPP-ET (F_{ET} , see text). The error bars are estimated from measures on different samples. The solid line is just a guide for the eye.

Table 1. Fitting Parameters of Normalized PL Traces Measured for the Donor–Ag–Acceptor Films with Different Ag Thickness and Control Samples

| sample | Ag thickness (nm) | A_1^a | t_1 (ns) ^a | A_2^a | t_2 (ns) ^a | A_3^a | t_3 (ns) ^a | F_{ET} (%) ^b |
|----------------|-------------------|---------|-------------------------|---------|-------------------------|---------|-------------------------|---------------------------|
| MEH-PPV-Ag | | 0.43 | 0.10 | 0.57 | 0.32 | | | |
| Ag-DPA | | 0.60 | 0.41 | 0.40 | 2.5 | | | |
| | 30 | 0.76 | 0.18 | 0.24 | 0.42 | <0.01 | 2.0 | 28 ± 8 |
| MEH-PPV-Ag-DPA | 60 | 0.53 | 0.18 | 0.42 | 0.54 | 0.05 | 2.2 | 64 ± 4 |
| | 100 | 0.27 | 0.18 | 0.65 | 0.53 | 0.08 | 2.5 | 66 ± 5 |
| | 150 | 0.24 | 0.18 | 0.66 | 0.51 | 0.10 | 2.3 | 51 ± 8 |

^aThe error on fitting parameters is estimated to be approximately 2% from residuals analysis. ^bCalculated as: $F_{ET} \approx (I_{DA} - I_A)/I_{DA}$. See text.

The simplest way to verify the presence of any kind of ET is the observation of the acceptor emission following the excitation of the donor. Figure 3b shows the PL spectra recorded for the control samples (donor-only, DPA/Ag/glass and acceptor-only, Ag/MEH-PPV/glass) and the analyzed multilayer structure DPA/Ag/MEH-PPV/glass with Ag thickness of 30 nm. A first rough estimate of the amount of energy transferred can be calculated comparing the areas under the spectra of Figure 3b. It is indeed possible to define the fraction of the total emission due to SPP-ET (F_{ET}) as $F_{ET} = (I_{DA} - fI_D - I_A)/I_{DA}$, where I_J ($J = D, A, DA$) is the area under the PL spectra of the DPA-only film ($J = D$), MEH-PPV-only film ($J = A$), and the complete multilayer structure ($J = DA$), respectively. f is a correction factor accounting for the decrease in the donor emission intensity in the donor–acceptor film with respect to the donor-only film. It is calculated as the ratio between the maximum PL intensity of D in the donor–acceptor and in the donor-only films.⁶ For the multilayer DPA/Ag/MEH-PPV/glass, the fraction of emission attributed to SPP-ET is about $23 \pm 6\%$. The uncertainty in these measurements is mainly connected with a precise determination of the f factor, strongly sample-dependent.

Although these measures give an immediate perception of the presence of SPP-ET, a more rigorous method to monitor the efficiency of the process is by means of time-resolved techniques, given that the lifetime of the donor is considerably longer than the acceptor one. In a time-resolved PL experiment, the temporal evolution of the spectrally resolved donor and acceptor emission is monitored. If the donor has a significantly longer lifetime than the acceptor, in the presence of ET a longer-lived PL for the acceptor should be recorded. The main advantage of time-resolved analysis is that moderate changes in the intensity of the excitation source or in the analyzed samples have a minimal effect on the PL dynamics.

Time-resolved emission data were collected for several samples having different Ag thicknesses (30, 60, 100, and 150 nm). Figure 4a shows the results obtained for a sample with a 60 nm Ag layer. By means of a suitable long-pass filter, only the PL in the spectral region dominated by the acceptor MEH-PPV emission was recorded ($\lambda > 610$ nm). Also in this case, the results obtained for the donor/Ag/acceptor films were compared to donor-only and acceptor-only control samples.

The donor-only response is at least 2 orders of magnitude weaker than the other samples because DPA emits very little in the selected spectral region, and it is strongly attenuated by the long-pass filter used in the detection apparatus. The acceptor-only response accounts for direct excitation of the MEH-PPV. Such contribution is significant for samples with thin Ag layers (30 and 60 nm), whereas thicker metal layers (100 and 150 nm) completely reflect the excitation beam preventing direct excitation of the MEH-PPV layer.

The temporal behavior of the depicted decay curves is quite complex because of the different local environment experienced by the excited molecules. The DPA-only films exhibit a double exponential decay with time constants 0.41 and 2.5 ns, in agreement with previous works on crystalline DPA films.^{37,39} The dynamics of MEH-PPV-only samples is characterized by a fast PL decay, with time constants of 100 and 320 ps.^{33,34,40} The presence of DPA donor on the other side of the Ag layer induces significant changes in the MEH-PPV dynamics, in particular the rise of long-lived components with time constants of 0.5 and 2.2 ns, similar to those found in the donor-only sample. As was already pointed out in refs 6, 22, this can be attributed to the presence of an SPP-ET, because it can be inferred that the long-lived acceptor emission is powered by the long-lived excited donors on the other side of the metal film. A careful analysis of all of the possible different relaxation pathways that could contribute to the final PL signal in the adopted experimental configuration is reported in the Supporting Information. Such analysis confirmed that the only non-negligible contribution is indeed SPP-ET.

It is also important to notice that the effect of the presence of the donor on the acceptor dynamics is strongly dependent on the Ag thickness. For the thinnest Ag layer (30 nm), the SPP-ET effect is strongly masked by the emission of MEH-PPV directly excited by the laser beam, whereas thick metal layers decrease the dipolar coupling strength and consequently the efficiency of the ET process.

Also in this case it is possible to determine a quantitative estimate of the efficiency of the SPP-ET in terms of the fraction of the total emission due to SPP-ET (F_{ET}), as defined above. In this case, I_J ($J = D, A, DA$) is defined as the area under the PL decays shown in Figure 4a. Moreover, given the experimental conditions, F_{ET} can be simplified as $F_{ET} \approx (I_{DA} - I_A)/I_{DA}$, because $I_D \ll I_{DA}$. The results obtained as a

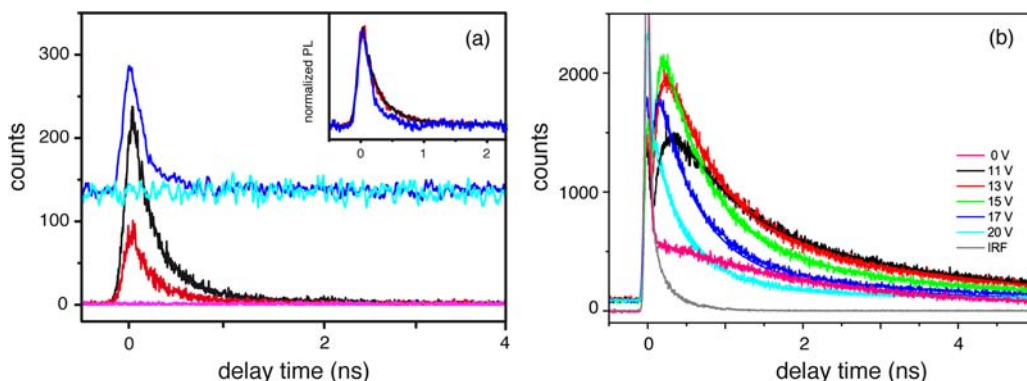


Figure 5. (a) Time-resolved luminescence of EPH1 [glass/ITO/PEDOT:PSS/MEH-PPV(80 nm)/Ag(100 nm)] at $\lambda > 610$ nm following direct photoexcitation of the MEH-PPV layer (black line, photoexcitation at 400 nm without applied bias; red line, photoexcitation at 400 nm and 5 V applied bias; blue line, photoexcitation at 400 nm and 16 V applied bias; cyan line, no photoexcitation and 16 V applied bias). The signal recorded in the absence of photoexcitation and applied bias is also shown for comparison (purple line). In the inset the normalized traces are reported for comparison. (b) Time-resolved luminescence of EPH2 at $\lambda > 610$ nm following photoexcitation of the DPA layer at different values of applied bias from 0 to 20 V.

function of Ag thickness are reported in the last column of Table 1 and in Figure 4b. Note that for the samples with Ag thickness of 30 nm, we found a value of F_{ET} in reasonable agreement with the one obtained integrating the static PL spectra of Figure 3b. The error bars in the values of F_{ET} (Figure 4b and last column of Table 1) are estimated from measures on different samples with the same structure.

Figure 4b shows that the transfer signal is most significant for intermediate silver thicknesses, peaking between 60 and 100 nm-thick films in which transfer accounts for more than 60% of the total emission. A similar behavior was found for SPP-ET associated with a different donor–acceptor pair and was ascribed to the nonmonotonic variation in dipolar coupling to the SPP modes.⁶ Closely related phenomena such as SPP-mediated transmission⁴¹ and emission⁴² of light through a metal film have similar dependences on metal thickness. The conditions leading to an optimum metal thickness for SPP-mediated phenomena are dictated by the particular nature of SPP modes acting at the two dielectric–metal interfaces.¹²

4.2. SPP-ET under Electrical Pumping. Once characterized, the SPP-ET process between MEH-PPV and DPA across an Ag film, the modifications to the photophysics, and dynamics of the process in the presence of an applied electric field were studied in an electrically pumped heterostructure (EPH). Given the emissive nature of MEH-PPV, the simplest heterostructure in which to study the effect of the simultaneous presence of optical and electrical excitation is an OLED-type structure. Typical MEH-PPV OLEDs were thus prepared: glass/ITO/PEDOT:PSS/MEH-PPV(80 nm)/Ag(100 nm) (hereafter referred to as EPH1). To obtain our prototype heterostructures, a further layer of DPA with thickness of 80 nm was grown on top of the Ag cathode (hereafter referred to as EPH2).

As preliminary characterization, the MEH-PPV luminescence properties of EPH1 samples were studied as a function of the applied bias. The results obtained with the TRPL technique are reported in Figure 5a. In the absence of any applied bias, photoexcitation at 400 nm of the MEH-PPV emitting layer results in the typical decay expected for MEH-PPV spin-coated films (black line), characterized by two time constants of approximately 0.1 and 0.3 ns (see Table 1 for comparison). In the presence of an applied bias below the turn-on threshold of the OLED, the yield of luminescence decreases (red line). When the applied bias is increased above the turn-on threshold, the presence of electroluminescence (EL) is manifested as a continuous background (cyan line). When a sufficiently strong voltage is applied, the quenching of PL is accompanied by a slight reduction of the time constant of the luminescence decay.

Figure 5b reports the results obtained for an EPH2 sample. Simulations reported in section 3 already predicted that the presence of further layers of ITO and PEDOT:PSS between the glass substrate and the acceptor layer does not alter the SPP-ET photophysics. This was also proven experimentally verifying that, within experimental

error, the time-resolved PL signal of several EPH2 prototypes in the absence of any applied bias and in the same experimental conditions was characterized by the same dynamics recorded for the model multilayer systems of Figure 4. The calculated F_{ET} resulted to be $71 \pm 6\%$, in good agreement with the value obtained for the model multilayer structure with 100 nm Ag layer.

On the other hand, it was also verified that in the absence of photoexcitation, EPH2 manifested the same electroluminescent behavior as EPH1. This confirmed that a further dye layer deposited on top of the metal cathode does not change in a significant way the outcoupling of the device (see also simulations in the Supporting Information).

When photoexcitation and a forward bias above the turn-on threshold are applied simultaneously, the recorded luminescence signal undergoes drastic changes. In particular, for applied voltages between 10 and 15 V, a striking enhancement of the signal amplitude is recorded. To quantify the amount of such enhancement, the luminescence signal obtained in the simultaneous presence of photoexcitation and applied electric field was compared to the pure PL signal (recorded at no applied bias) and with the pure EL signal (recorded in the absence of photoexcitation at different voltages). Figure 6a shows the overall luminescence (blue \blacklozenge), pure EL (green \blacksquare), and pure PL (pink \bullet) integrated signals, calculated as the area under the corresponding decays. Note that the pure PL signal does not carry any bias-dependence, being defined only at no applied bias (0 V). Therefore, in the enhancement calculation, its contribution has been considered constant (as shown by the pink line in Figure 6a). The figure reveals that, while the EL signal shows the typical saturation behavior as a function of applied voltage, the overall luminescence recorded in the simultaneous presence of an applied bias and photoexcitation shows instead a maximum around the EL saturation voltage (ca. 15 V). Furthermore, it is immediately noticeable that the contributions of EL and PL are not simply additive, and a net enhancement of the overall luminescence signal is recorded, as evidenced by the red trace in Figure 6a, calculated subtracting from the total luminescence the contributions of pure PL and EL at corresponding bias values. This behavior is well reproduced in several EPH2 samples prepared on different days.

The field-induced changes in the amplitude of the signal are also associated with different dynamics, mainly characterized by bias-dependent time constants and amplitudes. The decays reported in Figure 5b can indeed be fit as a sum of three exponentials plus an offset that takes into account the continuous contribution of EL. The results are reported in Figure 6. At all of the analyzed bias values, a component t_3 in the nanosecond range was recorded, whose amplitude is almost constant in the whole range of applied bias considered. The comparison with the dynamics of model multilayer structures of section 4.1 suggests that this component can be associated with the

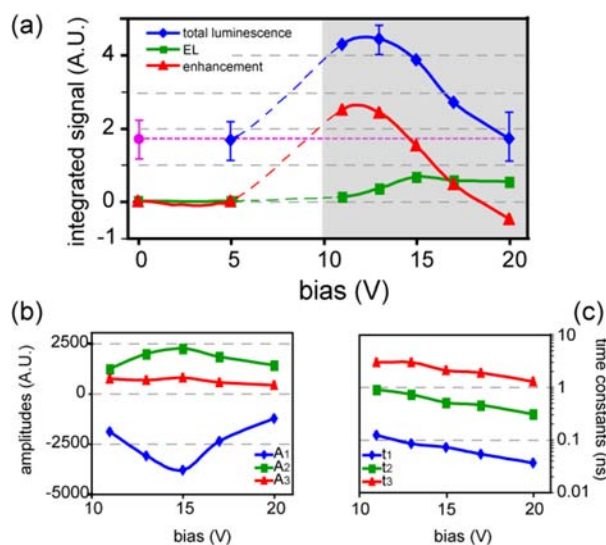


Figure 6. Dependence of the luminescence signal on the applied voltage for EPH2 samples. (a) Integrated electroluminescence (green ■) and total luminescence (blue ◆) signals as a function of the applied bias. The pure PL signal is defined only at no applied bias (pink ● at 0 V). The shadowed area indicates the range of voltage above the turn-on bias. For each voltage value, the net enhancement (red ▲) is calculated subtracting from the overall luminescence signal the contribution of the pure EL and PL. The error bars are estimated from repeated measurements on different devices. (b) Bias-dependent behavior of the amplitudes of the three time components defining the luminescence dynamics of EPH2. (c) Bias-dependent time constants (log scale). In all plots, the experimental points are joined by lines just to guide the eye.

direct emission of excitons generated through the SPP-ET from DPA to MEH-PPV. Beside the t_3 component, two subnanosecond components t_1 and t_2 were also detected, with time constants and amplitudes strictly dependent on the applied voltage (Figure 6b and c). While the time constants are shortened as the bias is increased, the amplitudes exhibit a more complex nonmonotonic dependence on the applied bias. This kind of response in general can be justified invoking the interplay of two kinds of processes having opposite dependence on the field. Interestingly, the fastest component (t_1) corresponds to a rise in the signal, and it appears only after the application of the external bias, which can thus be associated with the field-driven formation of photoluminescent species. The second component (t_2), characterized instead by positive amplitudes, can be associated with the decay of these species (see also the Supporting Information).

5. DISCUSSION

The results reported in Figures 5 and 6 clearly show that the presence of an SPP-ET from an antenna layer deposited on top of the metal cathode to the active luminescent MEH-PPV polymer leads to a striking enhancement of the luminescence performances of the device. In particular, the comparison of the luminescence decay traces of EPH1, having the typical OLED structure, and EPH2, showing SPP-ET, measured in the same experimental conditions (see blue traces in Figure 5a and b, respectively), reveals an enhancement of 1 order of magnitude in the luminescence performances. The most interesting characteristic of this phenomenon, never observed before, is the cooperative behavior of the electrical pumping and the SPP-ET process promoted by the photoexcitation of the antenna layer.

The voltage dependence of EPH2 luminescence is completely different from the trend observed for the conven-

tional OLED structures reported in this work (EPH1) as well as in previous literature.^{43–50} In effects, the luminescence response of MEH-PPV films encased in a diode structure as a function of the applied voltage has been the subject of intense investigation in the recent literature. Despite the variety of techniques used to investigate such effect and the different nature of the considered samples, all of these studies confirmed that the application of an electric field to a polymer film leads to luminescence quenching. There is now general consensus in attributing this phenomenon to the field-induced dissociations of excitons into e–h pairs. Some author also distinguished between amplitude and lifetime quenching based on whether a precursor to the emissive state or the emissive state itself is quenched by dissociation.^{48,49} In the first case, the luminescence quenching is due to a reduction of the concentration of emissive excitons, while in the second case it is due to their reduced lifetime. Moreover, when a forward bias is applied, the direct introduction of charge carriers (hole and electron polarons) provides a further quenching route for singlet excitons. The charge carriers possess indeed mid gap energy levels and therefore may accept energy from singlet excitons through Förster ET.⁵¹ This represents a further mechanism of lifetime quenching. These effects can be invoked to explain the field-dependent EPH1 luminescence (Figure 5a), in agreement with the literature previously cited. Such quenching mechanisms are acting also in EPH2: lifetime quenching is clearly proved by the bias-dependent decrease of the time constants described in the previous section, and amplitude quenching, which becomes predominant at high values of applied field, is likely responsible for the drop in the luminescence efficiency of EPH2 at biases >15 V. At lower voltages, the effect of lifetime quenching is neutralized by a bias-dependent amplitude enhancement. The interplay between these two effects with opposite outcomes on the final luminescence is responsible for the nonmonotonic dependence of the overall luminescence signal on the applied voltage.

The microscopic origin of the field-driven amplitude enhancement is not yet completely clear. The experimental data confirmed that this phenomenon is present only when an SPP-ET from an external antenna layer to the emissive polymer takes place. Moreover, the amplitude of the t_3 component, directly associated with the SPP-ET, remains almost constant in the whole range of potentials considered, suggesting that the dynamics of the ET itself is not much affected by the voltage. It is thus likely that the enhancement in the luminescence signal is associated instead with the particular dynamics and photo-physics of the excitations that this process generates in the MEH-PPV, and their interaction with the field and the charge carriers injected through the electrodes. In the adopted experimental conditions, the density of photoexcitations introduced by SPP-ET is indeed comparable with the density of charge carriers injected through the ITO (see the Supporting Information).

The SPP-ET process, as already demonstrated by TRPL data collected in model donor/Ag/acceptor multilayer structures in the absence of applied field, induces in the MEH-PPV film the formation of emissive species characterized by a longer luminescence behavior with respect to directly photogenerated excitons.

This results in an increased concentration of emissive long-lived species in the region immediately adjacent to the metal cathode and, in turn, in an altered equilibrium between the different neutral and charged excited species in this region. The

charge density in the vicinity of the metal cathode is particularly critical because EL, as a result of the reduced electron transport in the polymer film, originates from the recombination of holes and electrons confined in this region.⁵² It must be stressed that electronic charges in a conjugated polymer are not present as free electrons or holes, but as polaronic species.^{53–56} These species can have vastly different mobilities, always bias-dependent, and the equilibrium between them and neutral carriers like excitons is particularly sensitive to the applied field.⁵⁷ It can thus be supposed that the simultaneous injection of carriers by a suitable (<15 V) applied electric field and by SPP-ET nearby the metal cathode shifts the equilibrium carrier concentration so that the polaron holes, injected through ITO and traveling toward the cathode under the applied bias, experience a more favorable electron density, giving rise to a more efficient charge recombination farther from the cathode. This process would also explain the appearance of the two new time components t_1 and t_2 , compatible with the development of a new mechanism for the formation of emissive species. Our hypothesis seems to be supported also by the results of near-field scanning optical microscopy experiments conducted on MEH-PPV thin films, confirming the presence of local fluorescence enhancement under applied field in polymer films probed by biased optical microscope tips.^{58,59} Also, in that case the microscopic origin of the effect and the role of the electric field were not completely clear, although the authors suggested the presence of a field-induced variation of the concentration of carriers within the optical excitation volume. We could also exclude that the observed luminescence modulation is due to field-induced delayed fluorescence, already observed by other authors in conjugated polymers under pulsed⁶⁰ and static⁶¹ applied fields. The dynamics of such effect, controlled by the recombination of geminate pairs, is indeed too slow (in the order of some nanoseconds) to explain the time-resolved luminescence decays of Figure 5.

The applied electric field can strongly affect not only the mobility of the carriers introduced in the MEH-PPV by photoexcitation, but also their electronic and photophysical properties. Electroabsorption studies on conjugated polymers have demonstrated indeed that the application of an electric field can lead to a mixing of electronic states and a consequent shift of the absorption bands (Stark effect) and redistribution of the oscillator strength from allowed to forbidden transitions.⁵⁶ In the specific case of MEH-PPV films, the appearance of a broad weak feature on the blue side of the electroabsorption spectrum was associated with the field-induced activation of previously forbidden transitions.^{62,63} The field-induced increase of the absorption cross section on the blue side could affect the spectral overlap with the donor emission, increasing the efficiency of ET when the field is on. Furthermore, the field can act not only on electronic, photophysical, and mobility properties of the single layers, but can engage with the process of ET itself, promoting energy migration pathways otherwise forbidden (electric-field-induced-ET).^{64,65}

The experimental data do not allow estimating the real contribution of these effects on the final enhancement of luminescence, especially taking into account that in the experimental conditions adopted in this work, the positive bias applied to the sample to induce electroluminescence injects in the MEH-PPV film a remarkable amount of charged carriers (polarons), whose interactions with the photogenerated excitons are probably predominant. Further theoretical and experimental investigations are thus needed to clarify the real

origin of the recorded cooperative enhancement for applied bias <15 V and to verify the validity of the hypotheses proposed.

At high electric fields (>15 V), the density of the injected hole polarons become predominant with respect to the exciton density and their mobility increases. This probably favors ET from singlet excitons to the polaron band and accelerates lifetime and amplitude quenching mechanisms. Moreover, screening of the electric field due to the progressive accumulation of charges at the electrodes, causing an increase in the injection barrier and possible damage to the Ag electrode and emissive layer, must be taken into account.

6. CONCLUSIONS

Steady-state and time-resolved fluorescence techniques were employed to study and characterize the photophysics and the dynamics of ET processes mediated by surface plasmon polaritons (SPP-ET) with and without the application of an external field. The process was characterized in multilayer samples having the general structure: substrate/acceptor/Ag/donor, where the donor was a dye (DPA) and the acceptor an electroluminescent conjugated polymer (MEH-PPV). Preliminary simulations based on a classical dipole model and dyadic Green's functions approach were performed to calculate the energy flux within the structure and thus find the optimal donor–acceptor pair and the best multilayer design. The photoluminescence measurements, performed on samples with different Ag thicknesses ranging from 30 to 150 nm, confirmed the presence of SPP-ET processes leading to (i) an enhancement of the acceptor luminescence and (ii) a longer-lived dynamic behavior after donor excitation. The efficiency of the SPP-ET process, calculated as a fraction of luminescence due to SPP-ET (F_{ET}), depends on the metal thickness and reaches the outstanding value of $66 \pm 5\%$ for a 100 nm thick metal layer.

The possibility of exploiting such process to improve the performances of electrically pumped heterostructures like OPVs or OLEDs was then verified, studying the effects promoted by the application of external fields, invariably present during the operation of electrical devices. To this aim, electrically pumped heterostructures (EPH) were prepared replacing the glass substrate by an ITO glass, working as anode. The Ag layer served as metal cathode as well as plasmonic substrate to mediate ET when a further layer of the antenna dye (DPA) was included in the structure. Time-resolved luminescence decay traces of MEH-PPV in these structures under the simultaneous presence of SPP-ET process promoted by photoexcitation and electrical pumping are characterized by a striking enhancement of the overall luminescence in a wide bias range. Most interestingly, the electroluminescence promoted by the applied bias and the photoluminescence promoted by the SPP-ET are not simply additive, but the total recorded luminescence is greater than their sum, suggesting a cooperative behavior. The luminescence enhancement is also field-dependent, showing a nonmonotonic trend as a function of the applied bias with a maximum around the EL saturation voltage. On the basis of the luminescence dynamics, this field-dependent luminescence modulation was tentatively attributed to a field-induced variation of the concentration and lifetime of charged and neutral carriers within the electron–hole recombination volume.

In conclusion, the ability of modulating, and in particular of enhancing, the luminescence response of an electroluminescent device by means of SPP-ET is an extremely interesting result,

not so much as a mechanism to improve OLEDs performances, but rather as control mechanism. This introduces the possibility of inducing a detectable change in the device luminescence depending on the presence of a suitable dye capable to promote SPP-ET to the active medium. The availability of a light source whose output properties change in a controlled way depending on the substance present on its surface would allow for the realization of a new compact biosensor with integrated illumination.^{66,67} From this perspective, SPP-ET is particularly suited as controlling mechanism thanks to the extended range of ET (up to 100 nm) and its easy integration in the multilayer structure of conventional electrical devices.

■ ASSOCIATED CONTENT

■ Supporting Information

Further analysis of the experimental results and additional experimental data and simulations. This material is available free of charge via the Internet at <http://pubs.acs.org>.

■ AUTHOR INFORMATION

Corresponding Author

elisabetta.collini@unipd.it

Notes

The authors declare no competing financial interest.

■ ACKNOWLEDGMENTS

We would like to acknowledge financial support from the HELIOS Project (Università di Padova, Progetto Strategico 2008, prot. STPD08RCX). E.C. acknowledges the support of an "Assegno Senior" Fellowship from University of Padova. NSERC is thanked for financial support of preliminary work on this project.

■ REFERENCES

- (1) Hammarstrom, L.; Hammes-Schiffer, S. *Acc. Chem. Res.* **2009**, *42*, 1859.
- (2) Lu, Y.; Ogawa, K.; Schanze, K. S. *J. Photochem. Photobiol., C* **2009**, *10*, 173.
- (3) Scholes, G. D.; Fleming, G. R.; Olaya-Castro, A.; van Grondelle, R. *Nat. Chem.* **2011**, *3*, 763.
- (4) Atwater, H. A.; Polman, A. *Nat. Mater.* **2010**, *9*, 205.
- (5) Novotny, L.; Hecht, B. *Principles of Nano-Optics*; Cambridge University Press: Cambridge, 2006.
- (6) Andrew, P.; Barnes, W. L. *Science* **2004**, *306*, 1002.
- (7) Förster, T. *Discuss. Faraday Soc.* **1959**, *27*, 7.
- (8) Daniels, G. J.; Jenkins, R. D.; Bradshaw, D. S.; Andrews, D. L. *J. Chem. Phys.* **2003**, *119*, 2264.
- (9) Juzeliūnas, G.; Andrews, D. L. Quantum Electrodynamics of Resonance Energy Transfer. In *Advances in Chemical Physics*; Prigogine, I., Rice, S. A., Eds.; John Wiley & Sons: Hoboken, NJ, 2007; Vol. 112, p 1.
- (10) Lezec, H. J.; Thio, T. *Opt. Photon. News* **2004**, *15*, 29.
- (11) Weber, W. H.; Eagen, C. F. *Opt. Lett.* **1979**, *4*, 236.
- (12) Burke, J. J.; Stegeman, G. I.; Tamir, T. *Phys. Rev. B* **1986**, *33*, 5186.
- (13) Morawitz, H.; Philpott, M. R. *Phys. Rev. B* **1974**, *10*, 4863.
- (14) Chance, R. R.; Prock, A.; Silbey, R. Molecular Fluorescence and Energy Transfer near Metal Interfaces. In *Advances in Chemical Physics*; Prigogine, I., Rice, S. A., Eds.; Wiley: New York, 1978; Vol. 37.
- (15) Lakowicz, J. R. *Anal. Biochem.* **2005**, *337*, 171.
- (16) Economou, E. N. *Phys. Rev.* **1969**, *182*, 539.
- (17) Joseph, R. L. *Anal. Biochem.* **2001**, *298*, 1.
- (18) Lakowicz, J. R.; Ray, K.; Chowdhury, M.; Szmajcinski, H.; Fu, Y.; Zhang, J.; Nowaczyk, K. *Analyst* **2008**, *133*, 1308.

- (19) Mitamura, K.; Imae, T.; Tian, S.; Knoll, W. *Langmuir* **2008**, *24*, 2266.
- (20) Shimada, T.; Tomita, S.; Hotta, S.; Hayashi, S.; Yanagi, H. *Jpn. J. Appl. Phys.* **2009**, *48*, 042001.
- (21) Heidel, T. D.; Mapel, J. K.; Singh, M.; Celebi, K.; Baldo, M. A. *Appl. Phys. Lett.* **2007**, *91*, 093506.
- (22) Feng, J.; Okamoto, T.; Naraoka, R.; Kawata, S. *Appl. Phys. Lett.* **2008**, *93*, 051106.
- (23) Wang, Z. Y.; Chen, Z. J.; Xiao, L. X.; Gong, Q. H. *Org. Electron.* **2009**, *10*, 341.
- (24) Zhou, Z.-K.; Li, M.; Yang, Z.-J.; Peng, X.-N.; Su, X.-R.; Zhang, Z.-S.; Li, J.-B.; Kim, N.-C.; Yu, X.-F.; Zhou, L.; Hao, Z.-H.; Wang, Q.-Q. *ACS Nano* **2010**, *4*, 5003.
- (25) Celebi, K.; Heidel, T. D.; Baldo, M. A. *Opt. Express* **2007**, *15*, 1762.
- (26) Li, L. W.; Kooi, P. S.; Leong, M. S.; Yeo, T. S. *J. Electromagn. Waves Appl.* **1994**, *8*, 663.
- (27) Fitrilawati, F.; Tjia, M. O.; Pfeiffer, S.; Horhold, H. H.; Deutesfeld, A.; Eichner, H.; Bubeck, C. *Opt. Mater.* **2003**, *21*, 511.
- (28) Hashimoto, S.; Ohno, N.; Itoh, M. *Phys. Status Solidi B* **1991**, *165*, 277.
- (29) Zayats, A. V.; Smolyaninov, I. I.; Maradudin, A. A. *Phys. Rep.* **2005**, *408*, 131.
- (30) Pitarke, J. M.; Silkin, V. M.; Chulkov, E. V.; Echenique, P. M. *Rep. Prog. Phys.* **2007**, *70*, 1.
- (31) Collini, E.; Scholes, G. D. *J. Phys. Chem. A* **2009**, *113*, 4223.
- (32) Dykstra, T. E.; Kovalevskij, V.; Yang, X. J.; Scholes, G. D. *Chem. Phys.* **2005**, *318*, 21.
- (33) Samuel, I. D. W.; Crystall, B.; Rumbles, G.; Burn, P. L.; Holmes, A. B.; Friend, R. H. *Chem. Phys. Lett.* **1993**, *213*, 472.
- (34) Samuel, I. D. W.; Rumbles, G.; Collison, C. J.; Friend, R. H.; Moratti, S. C.; Holmes, A. B. *Synth. Met.* **1997**, *84*, 497.
- (35) Nijegorodov, N. I.; Downey, W. S. *J. Phys. Chem.* **1994**, *98*, 5639.
- (36) Hashimoto, S.; Ikuta, S.; Asahi, T.; Masuhara, H. *Langmuir* **1998**, *14*, 4284.
- (37) Williams, J. O.; Jones, A. C. *J. Lumin.* **1981**, *24–25*, 723.
- (38) Stevens, B. *Spectrochim. Acta* **1962**, *18*, 439.
- (39) Dutta, A. K.; Misra, T. N. *Opt. Mater.* **1994**, *3*, 35.
- (40) Smilowitz, L.; Hays, A.; Heeger, A. J.; Wang, G.; Bowers, J. E. *J. Chem. Phys.* **1993**, *98*, 6504.
- (41) Giannattasio, A.; Hooper, I. R.; Barnes, W. L. *Opt. Express* **2004**, *12*, 5881.
- (42) Winter, G.; Barnes, W. L. *Appl. Phys. Lett.* **2006**, *88*, 051109.
- (43) Khan, M. I.; Bazan, G. C.; Popovic, Z. D. *Chem. Phys. Lett.* **1998**, *298*, 309.
- (44) Kersting, R.; Lemmer, U.; Deussen, M.; Bakker, H. J.; Mahrt, R. F.; Kurz, H.; Arkhipov, V. I.; Bassler, H.; Gobel, E. O. *Phys. Rev. Lett.* **1994**, *73*, 1440.
- (45) Tasch, S.; Ekstrom, O.; Jost, T.; Scherf, U.; Leising, G. *Synth. Met.* **1997**, *85*, 1251.
- (46) Tasch, S.; Kranzelbinder, G.; Leising, G.; Scherf, U. *Phys. Rev. B* **1997**, *55*, 5079.
- (47) Deussen, M.; Haring Bolivar, P.; Wegmann, G.; Kurz, H.; Bassler, H. *Chem. Phys.* **1996**, *207*, 147.
- (48) Mehata, M. S.; Hsu, C.-S.; Lee, Y.-P.; Ohta, N. *J. Phys. Chem. B* **2010**, *114*, 6258.
- (49) Mehata, M. S.; Hsu, C.-S.; Lee, Y.-P.; Ohta, N. *J. Phys. Chem. C* **2009**, *113*, 11907.
- (50) Gulbinas, V.; Hertel, D.; Yartsev, A.; Sundstrom, V. *Phys. Rev. B* **2007**, *76*, 235203.
- (51) Arkhipov, V. I.; Emelianova, E. V.; Bassler, H. *Phys. Rev. B* **2004**, *70*, 205205.
- (52) Bozano, L.; Carter, S. A.; Scott, J. C.; Malliaras, G. G.; Brock, P. *J. Appl. Phys. Lett.* **1999**, *74*, 1132.
- (53) Frankevich, E. L.; Lymarev, A. A.; Sokolik, I.; Karasz, F. E.; Blumstengel, S.; Baughman, R. H.; Horhold, H. H. *Phys. Rev. B* **1992**, *46*, 9320.
- (54) Albrecht, U.; Bassler, H. *Chem. Phys. Lett.* **1995**, *235*, 389.

- (55) Barth, S.; Bassler, H. *Phys. Rev. Lett.* **1997**, *79*, 4445.
- (56) *Primary Photoexcitations in Conjugated Polymers: Molecular Excitation versus Semiconductor Band Model*; World Scientific: Singapore, 1997.
- (57) Petrovic, J. P.; Mataulj, P. S.; Pinto, L. R.; Zivanovic, S. R. *J. Nanophotonics* **2011**, *5*, 051808.
- (58) McNeill, J. D.; O'Connor, D. B.; Adams, D. M.; Barbara, P. F.; Kammer, S. B. *J. Phys. Chem. B* **2001**, *105*, 76.
- (59) McNeill, J. D.; O'Connor, D. B.; Barbara, P. F. *J. Chem. Phys.* **2000**, *112*, 7811.
- (60) Schweitzer, B.; Arkhipov, V. I.; Bassler, H. *Chem. Phys. Lett.* **1999**, *304*, 365.
- (61) Lupton, J. M.; Im, C.; Bassler, H. *J. Phys. D: Appl. Phys.* **2003**, *36*, 1171.
- (62) Martin, S. J.; Mellor, H.; Bradley, D. D. C.; Burn, P. L. *Opt. Mater.* **1998**, *9*, 88.
- (63) Martin, S. J.; Bradley, D. D. C.; Lane, P. A.; Mellor, H.; Burn, P. L. *Phys. Rev. B* **1999**, *59*, 15133.
- (64) Andrews, D. L.; Bittner, A. M. *J. Lumin.* **1993**, *55*, 231.
- (65) Andrews, D. L.; Crisp, R. G. *J. Fluoresc.* **2006**, *16*, 191.
- (66) Prasad, P. N. *Introduction to Biophotonics*; Wiley: New Jersey, 2004.
- (67) Shinar, J.; Shinar, R. *J. Phys. D: Appl. Phys.* **2008**, *41*, 133001.